Electronic Supplementary Material (ESI) for ChemComm.
This journal is © The Royal Society of Chemistry 2018

SUPPORTING MATERIAL - Table of content:

Supporting Notes:

Supporting Note 1:
The MPT domain is the direct counterpart to the KS domain in chain length control, and, as such, the ACP:MPT is a similarly relevant target for DDI engineering. However, the MPT domain is also responsible for loading malonyl, the elongation unit of FA synthesis, onto the ACP, and therefore acts in a dual manner on chain length control.[1-4] This makes the impact of ACP:MPT interface mutations more difficult to assess.
The strategy for engineering the ACP:MPT interface for the increased production of short acyl products was built on modulating mainly the elongation function of MPT. It is known from previous *in vitro* studies that a low ratio of malonyl-CoA to acetyl-CoA leads to short fatty acids, simply by increasing the chance of loading the priming acetyl into the fatty acid cycle.[1,3] In decreasing the ACP:MPT affinity, we expected to mimic a lowered malonyl concentration by a suppressed import of malonyl into the fatty acid cycle. Although a decreased affinity also weakens the release function of MPT, we assumed that a weakened interaction influences primarily the elongation, since the loading of malonyl is required in every elongation step (three times per C_8-CoA), while the release of the acyl moiety occurs just once per product.
Engineering of the ACP:MPT interface was guided by structural information available on the bacterial FAS type II systems from *Streptomyces coelicolor*.[5] Two residues in *C. ammoniagenes* FAS, R1494 and Q1647, were initially identified as candidate mutation sites. Given the general positive charge on the MPT surface around the entry to the active site (Fig. SI2), K1435 was chosen as another mutation site and exchanged in a second round of construct design. Here, also the active AT site was modified to transfer also short acyl chains and thus, potentially, act as an alternative exit pathway for product release.[3,6,7] With the AT modification, we aimed to untangle the dual role of MPT, so that the weakening of the ACP:MPT interface pronounces the targeting of the elongation function of MPT, since the AT "exit tunnel" for short acyl chains supports in the acyl chain release function. For this purpose, mutations I151A,[3] V289A, and L290A were introduced (see Table SI1).
Effects by MPT surface mutations were much less pronounced on both the product spectrum and the FAS activity (Fig. SI3, and Table SI1). This result may be explained by mutations that fail to throttle malonyl loading onto ACP to an extent that malonyl supply becomes a bottleneck in the fatty acid synthesis (under the chosen experimental conditions). Another explanation may be based on the dual function of MPT in malonyl loading and product unloading. Mutations may remain without significant effect, when both reactions are affected to a similar extent, and the AT modification is unable to rescue unloading by the alternative exit pathway.

Supporting note 2:
As can be observed from Fig. SI6 and SI7, the multiple sequence alignment indicates a target sequence deletion between S1434 and I1519 of the template KS (numbering as in 2UV8[8]) and an insertion located between the bacterial E1863 and D1878 of ACP (numbering as in UniProt database [9]). The secondary structure of the insertion was predicted using PSIPRED[10] as an α-helix between residues W1856 and G1867, followed by a loop conformation (Fig. SI8). The target structure was therefore restrained to an α-helix between A1854 (as informed by the template) and G1867. The non-DDI loop between R1869 and P1887 was replaced by three glycine residues.

Supporting note 3:
The mutation A2696K influences neither the FAS product spectrum nor its enzymatic activity. The residue 2696 is located at the periphery of the interface between ACP and KS. Despite a possible interaction between K2696 and N1776 (distance of 6.1 Å), the mutation does not trigger the modulation of both FAS function and DDI binding affinity (Fig. SI9).

Supporting note 4:
The effect of D2553A on the computed binding affinity is captured by combining the two alternative configurations of model A and model B. In such a scheme, R1754 is indeed a salt-bridge partner of D2553 (distance of 2.8 Å - Fig. SI10A). The increased hydrophobicity of A2553 repels the positive charge carried by 1754 (Fig. SI10B), affecting the orientation of the loop between K1752 and G1759 of ACP. The mutant interface increases FAS activity and the stability of the ACP:KS_2 complex. The mutation D2553N does not affect R1754 orientation and is entirely described by model B (Fig. S10C). Mutant N2553 introduces a change in charge that stabilizes the electrostatic network extended across ACP and KS.

Supporting note 5:
The mutation D2556A contributes indirectly to the stabilization of the complex interface and increases FAS activity. D2556 forms a salt-bridge with K1752 (distance of 2.7 Å) while electrostatic interaction is detected between R1774, N2557 and D2622 (Fig. SI11A). The hydrophobic mutant A2556 pulls K1752 towards the center of the interface. The additional negative charge strengthens electrostatic interactions increasing the stability of the complex (Fig. SI11B).

Supporting note 6:
Electrostatic interaction is detected between residues D2622, R1774 (distance of 5.4 Å) and Q2625 (distance of 6.1 Å). The dynamic of such network is not described by the static approach used to compute binding energies (Fig. SI12). The relative binding energy of D2622A therefore remains an outlier.

Supporting note 7:
We explored the possibility of competitive binding between ACP and either FAS^{GSMW} or a surface mutant using Monte Carlo (MC) simulation based on coarse-grained (CG) potential energies.[11] Relaxed homology models were taken from model set A. The protein domains were treated as rigid bodies described by one interaction site per residue located at the C_α atoms of the relaxed homology models. Considering only those mutant systems with severe impact on the FAS function, we compared FAS^{GSMW} to D2553A, D2556A, N2557E, N2621D, D2622A and, as control, to itself, resulting in six different examined constructs (Fig. SI13). The peripheral sides of the KS_2 Dimerization Motif 3 (DM3[12,13]) were located symmetrically facing each other and separated by 10 nm. Their relative positions were constrained by applying harmonic interaction potentials at the distance of the residues 2422 and 2509. ACP was placed at the center of mass of the construct, orthogonally to both KS dimers, and alternatively oriented towards the four productive DDIs. No constraint was applied on ACP. The investigated systems were solvated by a dielectric continuum with ε equal to 80 in a cubic box of 30 nm size (Fig. SI13). Conformations were sampled in $2.4*10^3$ independent MC simulations at the temperature of 300 K. For MC translational and rotational movements, we have used step sizes of 0.25 Å and 0.1 rad. A total of $2.4*10^8$ MC configurations was produced to exhaustively sample relevant interface conformations. In the attempt to characterize factors that affect the kinetic of association between ACP and KS_2, we analyzed the CG trajectories to quantify events of first encounter between the active site Ser1772 (ACP) and the enzymatic DDI residue Ser2766 (KS; as informed by the homology model A). In three different analyses, the number of first encounters were calculated by monitoring events of bound conformations. The proteins were considered bound if the two DDI interface residues were located within a distance of 8, 10, and 12 Å. We used the python libraries MDAnalysis[14,15] and SciPy[16] to derive the relative CG bead positions and to perform the distance matrix computations, respectively. Depending on the impact of the DDI perturbation on product length and binding free energy, we expected ACP to preferentially interact either with FAS^{GSMW} or the surface mutants, resulting in corresponding shifted first encounters distributions for the mutant D2553A and D2556A (ACP:mutant high relative interaction frequency) and for N2557E, N2621D and D2622A (ACP:mutant low relative interaction frequency). As illustrated in Fig.

SI14, D2553A shows the largest fluctuation of first encounter events (eleven events counted within a threshold of 12 Å), which is however not statistically relevant. The CG analysis does, overall, not lead to statistically conclusive results, which may be interpreted by challenges in simulated binding kinetics in a confined environment and the lack of experimental data on the structure of *C. ammoniagenes* FAS. Nevertheless, the reduced representation of the system may enable the investigation of the entire *C. ammoniagenes* cage-like FAS machinery and the enhanced sampling of productive interactions between ACP and the catalytic components. Such an approach could be therefore resumed in the light of new structural information on *C. ammoniagenes* FAS.

Supporting Methods:

Cloning. FAS from *C. ammoniagenes* was initially cloned into a pET-22b(+)vector (Novagen, Merck Millipore).[17] It was constructed with an N-terminal strep twin tag with short linker (MSAWSHPQFEKGGGSGGGSGGSAWSHPQFEKGAGS) or the shorter version, the strep II tag (MSAWSHPQFEKGAGS).[18]

For the introduction of point mutations, site directed mutagenesis was used and vectors were linearized via PCR in which primers carried the mutation (for primers, see Supplementary Note 1). After digestion with Dpn1 (New England Biolabs), a preparative agarose gel (0.8%) was run and the DNA extracted from the latter. The linearized vectors were transformed into competent *E. coli* cells (Stellar cells, Clontech) according to the manufacture's protocol and amplified. All constructs were sequenced for correct incorporation of the mutation.

For later co-transformation with *C. ammoniagenes* FAS AcpS (for posttranslational addition of phosphopantetheine on the FAS), AcpS was cloned (for primers, see Supplementary Note 1) into a pETcoco vector (Novagen, Merck Millipore) and amplified.

Primers used for introduction of point mutations and AcpS cloning. The initial cloning of *C. ammoniagenes* FAS was done in a previous study.[3] Its primers for Infusion cloning into pET-22b(+)vector were included here for completeness (15 bp overlap with vector ends at the 5' end, underlined). Initial construction of the insert included approximately 270 bp after the actual stop codon since the gene was wrongly annotated in databases.

fwd 5' AAAAGGCGCCGGATCCACTATTGGCATCTCTAACCACCGCCTGG 3'
rev 5' GGTGATGATGCTCGAGCTGGTGGCTTGCCGTAGATCGCTTGC 3'

Reference FAS with a double mutation in the KS domain (G2599S M2600W)

fwd 5' CCCAGGGCACG**AGTTGG**GGCGGCATGCAGTCGATGCGC 3'
rev 5' GCGCATCGACTGCATGCCGCC**CCAACT**CGTGCCCTGGG 3'

For the introduction of the point mutations on the surface of the domains, complimentary pairs of primers were designed. The PCR was used to amplify and linearize the whole vector. In primers, underlined parts are indicating the overlap of primer pairs while mutation sites are in bold. The domain, purpose and exact residue are listed for each primer.

KS domain, surface modulation:

D2553A fwd 5' CCGGCC**GCT**ATGATTGACAACCTCGACCGG 3'
D2553A rev 5' AATCAT**AGC**GGCCGGAATACCGTAGACACCGG 3'
D2553N fwd 5' CCGGCC**AAT**ATGATTGACAACCTCGACCGG 3'
D2553N rev 5' AATCAT**ATT**GGCCGGAATACCGTAGACACCGG 3'
D2556A fwd 5' CCGGCCGATATGATT**GCA**AACCTCGACCGGGTGGCCTTGTGG 3'
N2557A fwd 5' CCGGCCGATATGATTGAC**GCA**CTCGACCGGGTGGCCTTGTGG 3'
N2557E fwd 5' CCGGCCGATATGATTGAC**GAA**CTCGACCGGGTGGCCTTGTGG 3'
D2556 N2557 (for both sites) rev 5' AATCATATCGGCCGGAATACCGTAGACACCGG 3'
N2621A fwd 5' GCGCAGCCGCGCCCG**GCT**GACATCTTGCAGGAAGCACTGCCG 3'
N2621D fwd 5' GCGCAGCCGCGCCCG**GAT**GACATCTTGCAGGAAGCACTGCCG 3'
D2622A fwd 5' GCGCAGCCGCGCCCGAAT**GCA**ATCTTGCAGGAAGCACTGCCG 3'
N2621 D2622 (for both sites) rev 5' CGGGCGCGGCTGCGCCAG 3'
A2696K fwd 5' GGCTTCGGCGATATG**AAA**GCCACGGCGGATTCCGGC 3'
A2696 rev 5' CATATCGCCGAAGCCCGTAATGCC 3'

MPT domain, surface modulation:

K1435A fwd 5' CGAAT**GCG**ATTGGCATCCGCGCCGAGGACG 3'
K1435A rev 5' GCCAAT**CGC**ATTCGGGCGCAGCGCTGCCAG 3'
R1494A fwd 5' GCATG**GCC**TCATTTATCATGATCCCGGGCATCGACG 3'
R1494A rev 5' TAAATGA**GGC**CATGCCCGGCGCGCGCGAC 3'
Q1647A fwd 5' CTCGGC**GCA**ACCCTGCGCTTGCCGCAATACGC 3'
Q1647A rev 5' CAGGGT**TGC**GCCGAGCATATTCGCAAGCGTCGG 3'

AT domain, binding channel:

I151A fwd 5' CAGCTC**GCC**GGCGTCGCTATTTCTAAG 3'

I151A rev 5’ GACGCC**GGC**GAGCTGCGCCAGCGCAATAAC 3’
V289A fwd 5’ GATGGCGCAGAGGCA**GCC**TTGACGGAGATCGTGAACTGGCC 3’
L290A fwd 5’ GATGGCGCAGAGGCAGTC**GCA**ACGGAGATCGTGAACTGGCC 3’
V289A L290A fwd 5’ GATGGCGCAGAGGCA**GCCGCA**ACGGAGATCGTGAACTGGCC 3’
V289 L290 rev 5’ TGCCTCTGCGCCATCGTGAGCC 3’

For cloning of *C. ammoniagenes* FAS AcpS into a pETcoco vector, the following primers were used. The overlap to the vector is underlined, the parts binding the genomic DNA for the insert amplification are shown in bold.
fwd 5’ AGAAGGAGATATAAGC**ATGCTCGACAACCGTGAAGCGATGAC** 3’
rev 5’ TCGAGTGCGGCCTAGG**TTACCGCTGGTACCGCAGCAGG** 3’

Expression. For the expression, both the plasmid carrying the *C. ammoniagenes* FAS construct and the plasmid of the *C. ammoniagenes* FAS AcpS were co-transformed into *E. coli* competent cells (BL21 (DE3) gold, Agilent Technologies) according to the manufacture’s protocol, plated on LB+1.5% agar (with 50 µg mL^{-1} ampicillin, 11 µg mL^{-1} chloramphenicol, 0.01% arabinose final concentration) and grown over night at 37 °C. A colony was picked and grown in a preculture (LB media with 100 µg mL^{-1} ampicillin, 34 µg mL^{-1} chloramphenicol and 0.01% arabinose) at 37 °C over night. The preculture was transferred into the main culture of TB media (also containing 100 µg mL^{-1} ampicillin, 34 µg mL^{-1} chloramphenicol and 0.01% arabinose). The culture was grown at 37 °C with 180 rpm shaking until an OD_{600} of 0.8 was reached. The culture was then cooled down to 20 °C and shaken at this temperature for 30 min before IPTG addition (final concentration 250 mM). Cultivation was continued over night at 20 °C. The cells were harvested by centrifugation at 4,000 rcf for 20 min. The wet cell pellet weight was typically around 20 g L^{-1} of TB culture. If the cells were not further processed directly, they were flash frozen in liquid N_2 and stored at -80 °C.

Protein purification. The protein was purified similar as described before.[4] For protein purification, buffer W (100 mM Na_2HPO_4/NaH_2PO_4, pH 7.2, 100 mM NaCl, 1 mM EDTA) was added to the cell pellet to a total volume of 35 mL. After addition of 2 mg of DNAse I (AppliChem) and protease inhibitor (complete EDTA-free, Roche, Mannheim, Germany), the cells were resuspended by stirring. French press was used to lyze cells (16 000 psi). Cell lysates were kept at 4 °C to avoid protein degradation. After centrifugation (60,000 rcf for 60 min), the supernatant (approx. 30 mL) was transferred onto a strep column (5 mL resin volume, IBA) followed by 8 column volumes (CV) of washing. The protein was eluted with 3 CV buffer E (same as buffer W but with 2.5 mM D-desthiobiotin). After SDS-PAGE analysis, promising fractions were pooled and concentrated in a centrifugal filter (100,000 nominal molecular weight limit, Amicon Ultra-4, Merck Millipore).
In a next step, the proteins were purified by size exclusion chromatography (column: Superose 6 10/300GL, GE Healthcare, buffer G: 100 mM Na_2HPO_4/NaH_2PO_4, pH 7.2, 100 mM NaCl) and were checked for the desired hexameric oligomers. Those fractions were again pooled using a centrifugal filter to a concentration of 10 – 20 mg mL^{-1} of protein. To compensate a potential loss of FMN, a five fold molecular excess of FMN was added to the protein sample. Samples were then mixed with glycerol (final concentration 50%) and stored at –20 °C. Glycerol does not have an effect on product distributions as shown previously.

Activity assay. The activity assays were performed as described before with buffer AB (400 mM KH_2PO_4/K_2HPO_4 pH 7.3, 3.5 mM DTT), 50 nmol acetyl-CoA, 30 nmol NADPH and 25 µg of the FAS protein.[3] After initial recording of the absorption at 334 nm for some time, 60 nmol malonyl-CoA were added to start the reaction. The corrected rate of NADPH absorption (measured rate minus rate prior to malonyl-CoA addition) was calculated and the activity determined. Activity of each purified protein was determined in three relicates.

Product assay. The product assays were performed as described before.[3] The reaction volume of 100 µL contained 90 µL of master mix (consisting of 50 µL of buffer AB, described above; 20 nmol acetyl-CoA, 100 nmol malonyl-CoA, 225 nmol NADPH all dissolved in water) and 20 µg of purified FAS. The reaction mix was incubated at room temperature for 4 hours. Then, 440 µL of acetone (cooled in ice bath) and the internal standards ($isoC_5$-CoA and C_{17}-CoA, final concentration 50 µM;

in C_n-CoA, n represents the number of carbons in the acyl chain) were added and the mix was vortexed for 20 s. The reactions were stored at -20 °C over night for precipitation of proteins and salts. The mixture was then centrifuged at 0 °C for 5 min at 20,000 rcf. Directly afterwards, 500 µL of supernatant were transferred to a new vial and evaporated to dryness under reduced pressure using a SpeedVac. Pellets were redissolved in 40 µL water by sonification for 5 min. After another centrifugation step (5 min at 20,000 rcf), samples were transferred into sample vials and measured via HPLC-UV-MS.

HPLC quantification. The acyl-CoA esters were analyzed on a HPLC (Dionex Ultimate 3000 RSLC) coupled to an ESI-TOF mass spectrometer (Bruker micrOTOF-Q II). For chromatographic separation an RP-18 column (100 x 2.1 mm, particle size 1.7 µm, Waters Acquity BEH) was used with a mobile-phase system of buffer A (water, 10 mM triethylamine/acidic acid buffer, adjusted to pH 9.0) and buffer B (acetonitrile). A multistep gradient at a flow rate of 0.25 mL min^{-1} was used. The starting condition of buffer B was at 7%, followed by a linear increase to 60% until 6 min, then to 70% until 9.5 min and finally to 90% until 10 min runtime. Data were acquired in negative mode in a scan range from 200–2000 *m/z.* For quantification, the UV trace at 260 nm was analyzed using DataAnalysis 4.0 software (Bruker Daltonik). For calibration C_6-CoA, C_8-CoA, C_{10}-CoA, C_{12}-CoA, C_{14}-CoA, C_{16}-CoA, C_{18}-CoA as well as the internal standards iC_5-CoA and C_{17}-CoA were measured. Calibration points were measured three times each for 10 pmol, 25 pmol, 50 pmol, 100 pmol, 200 pmol, 1000 pmol and 2000 pmol. Included in the calibration range were only average signals that did not differ from their calculated value more than 20%.

Protein sequence alignment. We performed a full-length sequence alignment of *C. ammoniagenes* fatty acid synthase (FAS, UniProt code: Q04846) to 29 bacterial and eukaryotic FAS sequences collected from ref[19] and ref[12]. All considered sequences were retrieved in FASTA format from UniProt[9] and aligned using the web-server software MAFFT version 7[20]. We performed the alignment using the iterative refinement method FFT-NS-i with BLOSUM62 scoring matrix[21] and a gap opening penalty of 1.53. The full-length alignment was visualized in JalView[22].

Protein homology modeling. We constructed KS:ACP_2 homology models using the software MODELLER version 9.16.[23] The X-ray crystallographic structure of *S. cerevisiae* FAS (2uv8[8]) was used as template. Yeast ACP carries a 4'-phosphopantetheine (Ppant) arm attached to S180. Ppant is distant from the introduced surface point mutations and it was therefore excluded from the modelling process (Fig. SI4). Different to bacterial ACP,[24,25] yeast ACP does not engulf the acyl-chain,[26] so that the Ppant and the acyl-chain (and the variations of the acyl-chain in length and β-carbon decoration) were expected to have little impact on calculated relative binding energies. Secondary structure restraining was performed using the automodel.special_restraints routine of MODELLER (details can be found in note SI2).

We constructed two different sets of models (A and B) each containing $2*10^3$ alternative configurations. Set A displayed template loop features. Set B provided alternative conformations of the non-conserved and flexible DDI loop between K1752 and G1759 of ACP. The possibility of interaction between R1754 and D2553 was investigated by evaluating all B structures according to their R1754 side-chain orientations. Arginine orientations capable of forming the salt bridge were filtered by accepting only models in which the charged atoms of R1754 and D2553 were located within 3 Å. In the two sets, the wild type homology models (Model A and Model B) were then selected based on their discrete optimized protein energy (DOPE) score. The point mutations were introduced using MODELLER, resulting in two different series of ten models each**.** Chimera software was used for structure visualizations[27].

MD simulations. We energy minimized and MD equilibrated the selected *C. ammoniagenes* ACP:KS_2 homology models using the molecular dynamics package GROMACS version 5.1.4 and the force field CHARMM36 (version Nov2016).[28-30] To mimic neutral pH conditions, aspartates and glutamates were negatively charged, lysine and arginine positively charged, and histidines neutral. The N-terminus and C-terminus were capped with ACE and NME groups, respectively. The protein complexes were then solvated in a cubic box of size 12.3 nm^3 with 0.1 M NaCl aqueous solution,

maintaining overall charge neutrality. For each model, high energy interactions and possible steric clashes were relaxed through 50,000 steepest-descent energy minimization steps, or until the maximum force dropped below 200.0 kJ mol^{-1} nm^{-1}. The energy-minimized systems were equilibrated in 5 ns of NVT MD simulation, followed by 20 ns of NPT MD simulation. All simulations were performed at a temperature of 300 K and a pressure of 1 bar. Temperature and pressure were controlled by applying V-rescale[31] and Parrinello-Rahman algorithms, respectively.[32] All trajectories were visualized using the software VMD[33].

Binding energy computations. We used the molecular mechanics Poisson-Boltzmann surface area (g_MMPBSA) software[34] to compute DDI binding energies of the ACP:KS_2 homology models. The tool g_MMPBSA computes the binding energy of protein complexes based on the evaluation of molecular mechanical, polar and apolar solvation energies. Molecular Mechanical (MM) energies depend on electrostatic (E_{elec}) and van der Waals (E_{vdW}) contributions. The computation of polar solvation energies was performed using the Assisted Poisson-Boltzmann Solver (APBS).[35] The apolar solvation energy contributions are calculated exploiting the Solvent Accessible Surface Area (SASA) model.[36,37] Binding free energies are represented as the difference between bound and free states,

$$\Delta G_{binding} = G_{complex} - \left(G_{KS_2} - G_{ACP}\right)$$

where the free energy contributions of the complex and its isolated components are decomposed into a sum of molecular-mechanics, solvent, and configurational entropy contributions,

$$G = \Delta E_{MM} + \Delta G_s - T\Delta S = \Delta E_{(bonded\,+\,non-bonded)} + \Delta G_{(polar\,+\,non-polar)} - T\Delta S$$

The binding energy evaluations were performed on thirty-five frames extracted at 0.5-ns intervals from the final 17 ns of NPT MD simulations of the homology models. Binding affinities were computed by averaging the thirty-five energy contributions. Differences in binding affinity were calculated between DDI surface mutants and FAS^{GSMW}. This double-differencing scheme aims to minimize systematic errors caused by possible model inaccuracy and incomplete sampling.

Supporting Figures and Table:

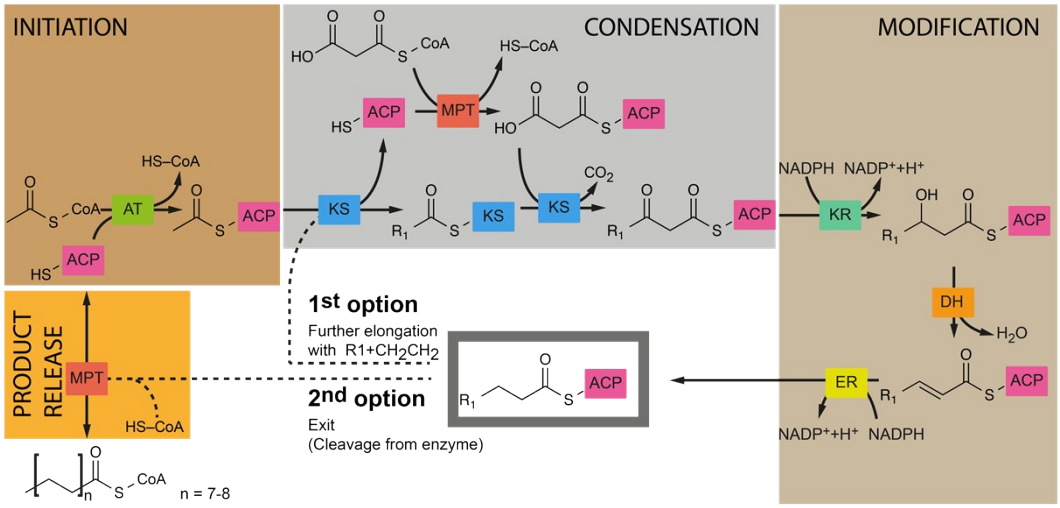

Figure SI1. Reaction scheme of FAS on the example of microbial type I synthesis. FA synthesis is initiated with the loading of the acyl carrier protein (ACP) with acetyl catalyzed by the acetyl transferase (AT). For condensation, acetyl (or in later cycles, the acyl) is transferred onto the ketoacyl synthase domain (KS). Free ACP is then loaded with malonyl by the malonyl/palmitoyl transferase (MPT) domain Malonyl is condensed by KS with acetyl to form the β-ketoester while releasing CO_2. The β-keto intermediate is successively modified by ketoacyl reductase (KR), dehydratase (DH) and enoyl reductase (ER). The fully reduced acyl chain then starts the cycle again and can either be elongated again (1st option) or unloaded from ACP by the MPT domain (2nd option).[38] Typically, fatty acids with a length of 16 or 18 carbon atoms are produced.

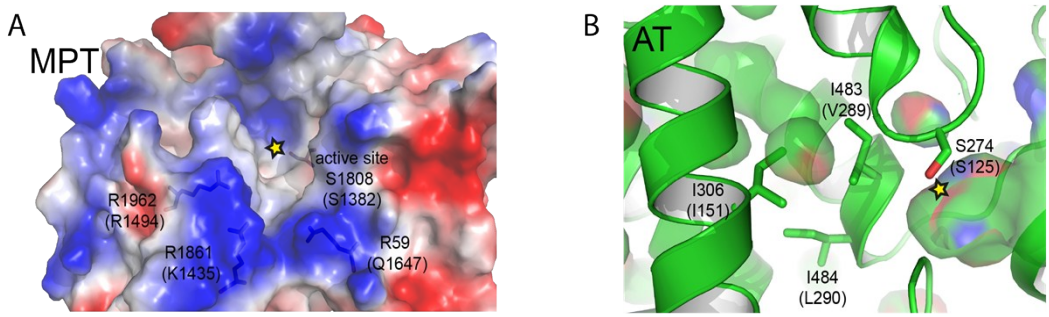

Figure SI2. Engineering of transferases. (A) The MPT domain surface representation is shown with vacuum electrostatics indicated. The active site and residues that were mutated are shown in their native form. (d) The AT binding site is shown in cartoon representation with the active site and the mutation sites in stick representation. The active site is loaded from the right (surface of entrance channel shown). With the introduction of the mutations, a binding channel presumably opens up extending to the top left.

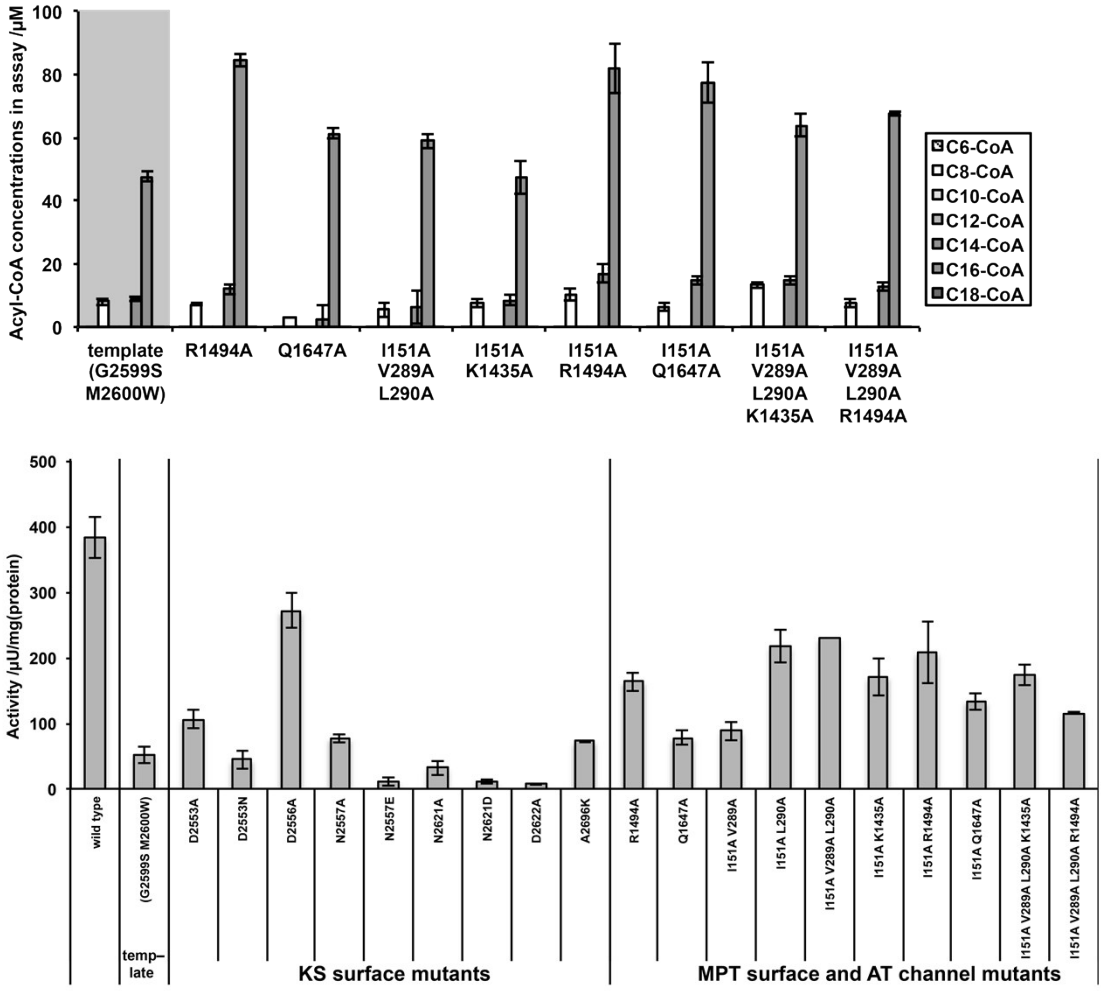

Figure SI3. Product spectra of MPT surface mutation (K1435A, R1494A, Q1647A) and AT binding channel mutations (I151A, V289A, L290A) are shown, also in combinations thereof. As for the KS surface mutants, all mutations were introduced in the test FAS carrying a G2599S M2600W mutation already. Error bars show the standard deviation of three assays for each construct. Selected mutants have been tested in biological replicates. (c) Overall fatty acid synthetic activities of FAS constructs. The activities of the FAS constructs were measured by NADPH consumption.[3] One unit (U) is defined as the incorporation of 1 µmol of malonyl-CoA per minute. Wild type and the template are shown for comparison. MPT/AT mutants also carry the template mutations (G2599S M2600W), which has not been stated in the figure explicitly. Error bars show standard deviation from three measurements for each protein.

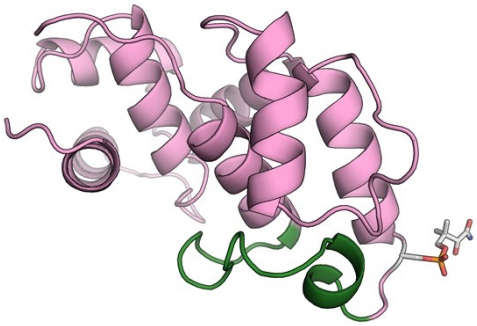

Figure SI4. Representation of the ACP protein structure with Ppant attached to S180 of ACP (pdb: 2uv8[8]). The modification does not influence the investigated domain-domain interface and was therefore not modelled. All local template features influenced by the post-translational modification are however reflected by the structure of the target.

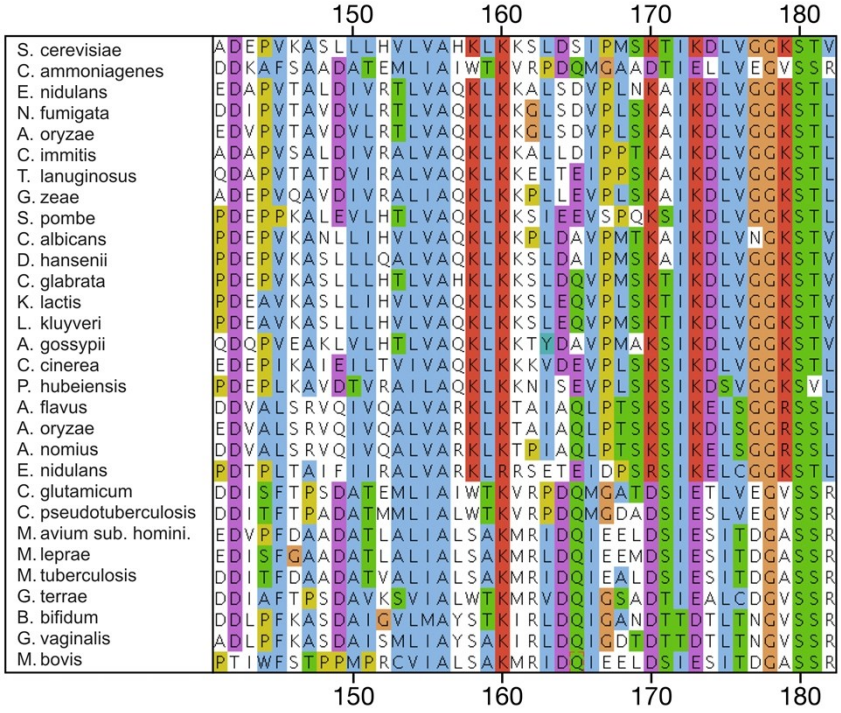

Figure SI5. Section of the full-length multiple sequence alignment of FAS highlighting the loop located between K160 and P167 of ACP (numbering as in 2uv8[8] and CLUSTAL X coloring scheme[39]). The sequence of the template (*S. cerevisiae*) and the target (*C. ammoniagenes*) are listed in the first and second rows. The multiple sequence alignment indicates that target loop residues V1753 and R1754 correspond to template K161 and S162, respectively.

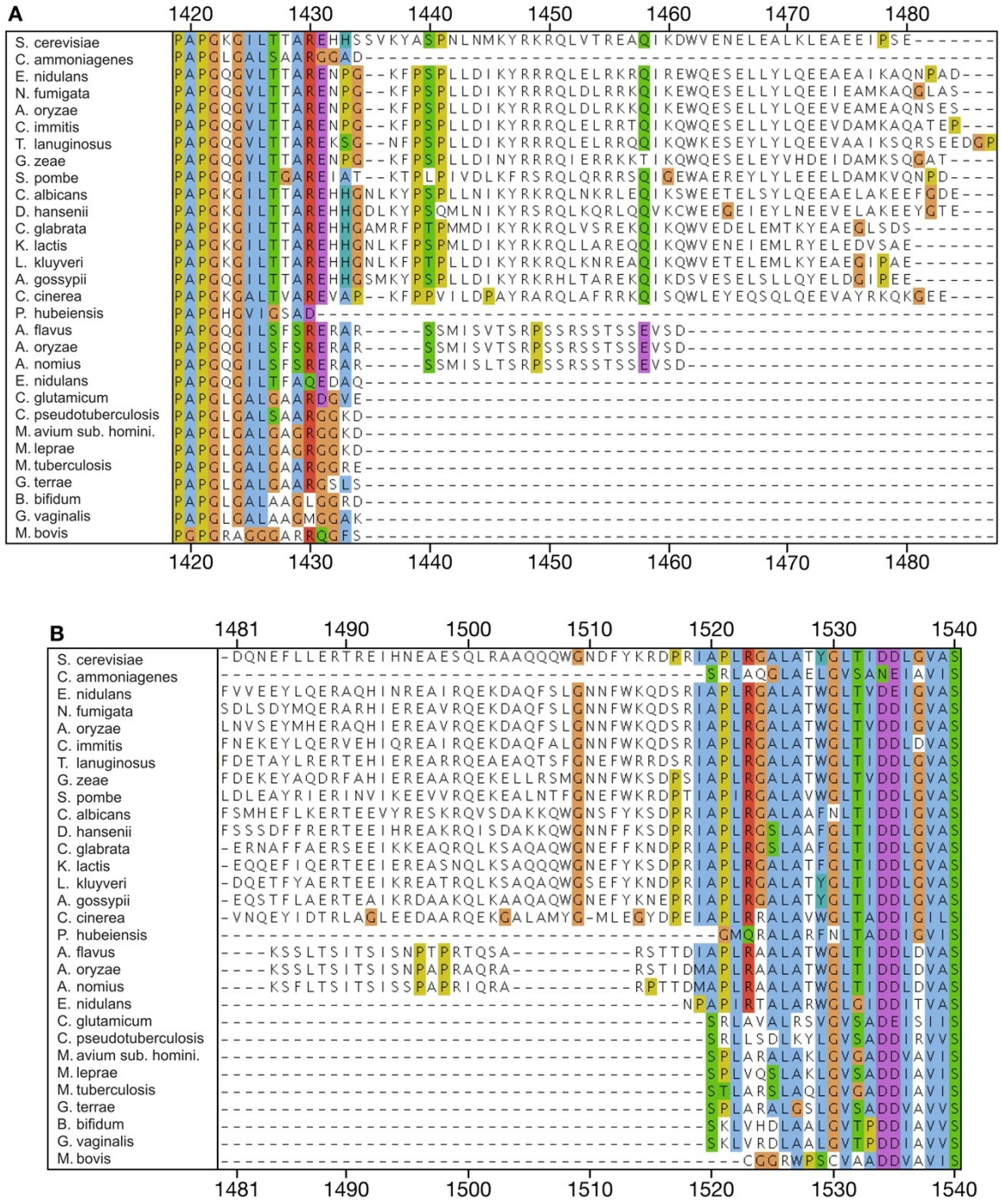

Figure SI6. Section of the full-length multiple sequence alignment of FAS highlighting the target sequence deletion between S1434 and I1519 of the template KS (numbering as in 2uv8[8] and CLUSTAL X coloring scheme[39]). The sequence of the template (*S. cerevisiae*) and the target (*C. ammoniagenes*) are listed in the first and second rows. (A) Sequence alignment between the template residues 1419 and 1480. (B) Sequence alignment between the template residues 1481 and 1540.

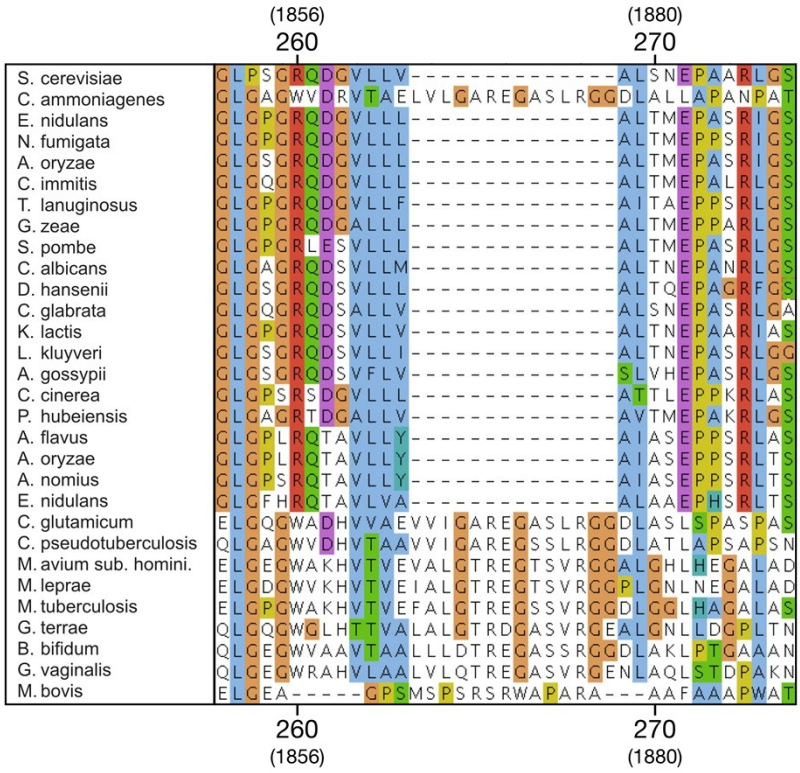

Figure SI7. Section of the full-length multiple sequence alignment of FAS highlighting the target sequence an insertion located between the bacterial E1863 and D1878 of ACP (numbering as in 2uv8[8] and CLUSTAL X coloring scheme[39]). The sequence of the template (*S. cerevisiae*) and the target (*C. ammoniagenes*) are listed in the first and second rows.

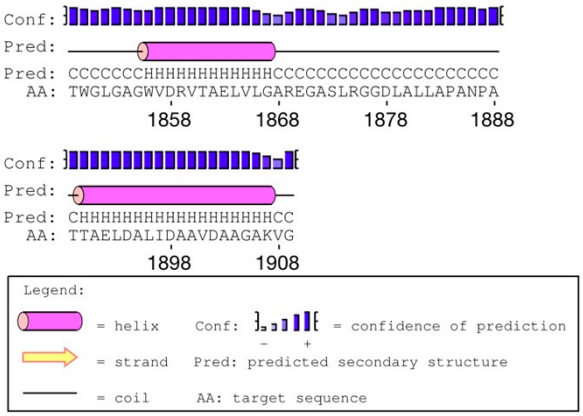

Figure SI8: Secondary structure PSIPRED predictions of the *C. ammoniagenes* ACP region between 1849 and 1909 (H = helix, C = coil). The confidence of the prediction is illustrated in blue histograms.

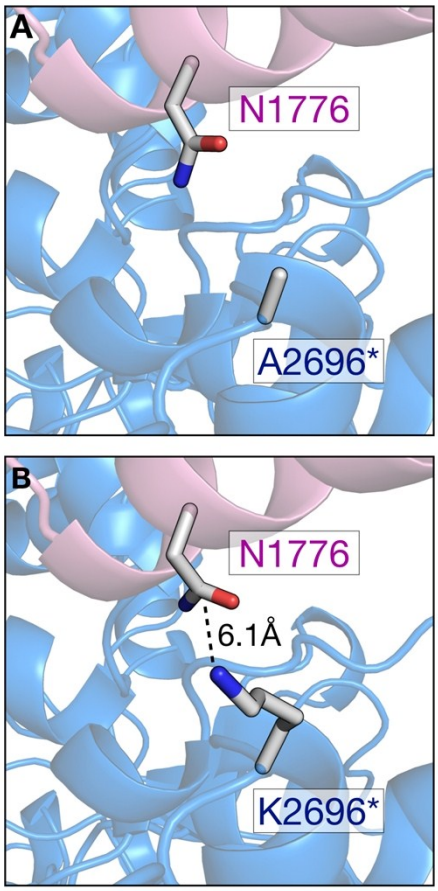

Figure SI9. Close-up of the interface across KS and ACP. KS, ACP residues and atom distances are highlighted in blue, magenta and black, respectively. Dashed lines indicate interaction between residues. The point mutation sites are marked with a star. (A) Wild-type interface with residues A2696 and N1776. (B) Mutant interface with residues K2696 and N1776, illustrating possible electrostatic interaction at a distance of 6.1 Å.

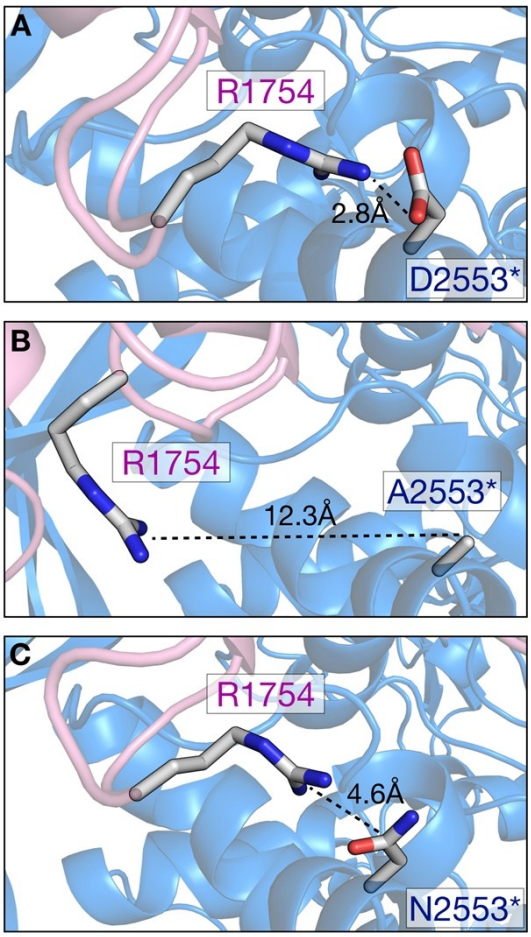

Figure SI10. Close-up of the interface across KS and ACP. KS, ACP residues and atom distances are highlighted in blue, magenta and black, respectively. Dashed lines indicate interaction between residues. The point mutation sites are marked with a star. (A) Wild-type interface with residues D2553 and R1754, stabilized by a salt-bridge (distance of 2.8 Å). (B) Mutant interface with residues A2553 and R1754. The apolar mutant repels R1754, increasing the distance to 12.3 Å. (C) Mutant interface with residues N2553 and R1754. The polar mutant does not affect R1755 orientation and an electrostatic interaction is detected at a distance of 4.6 Å.

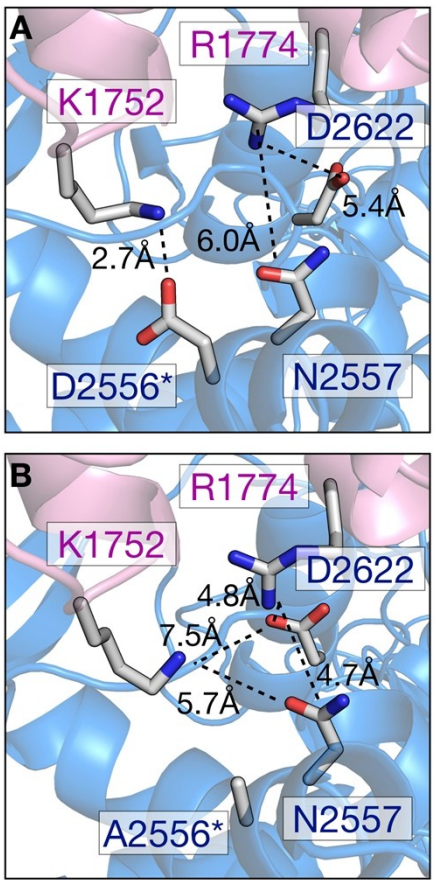

Figure SI11. Close-up of the interface across KS and ACP. KS, ACP residues and atom distances are highlighted in blue, magenta and black, respectively. Dashed lines indicate interaction between residues. The point mutation sites are marked with a star. (A) Wild-type interface with residues D2556, N2557, D2662, K1752 and R1774. D2556 forms a salt-bridge with K1752 at a distance of 2.7 Å. Electrostatic interaction is detected between K1772, N2557 (distance of 6.0 Å) and D2662 (distance of 5.4 Å). (B) Mutant interface with residues A2556, N2557, D2662, K1752 and R1774. As the hydrophobic mutant pulls K1752 towards the interface core, stronger interaction is detected between R1774, N2557 (distance of 4.7 Å) and D2662 (distance of 4.8 Å)

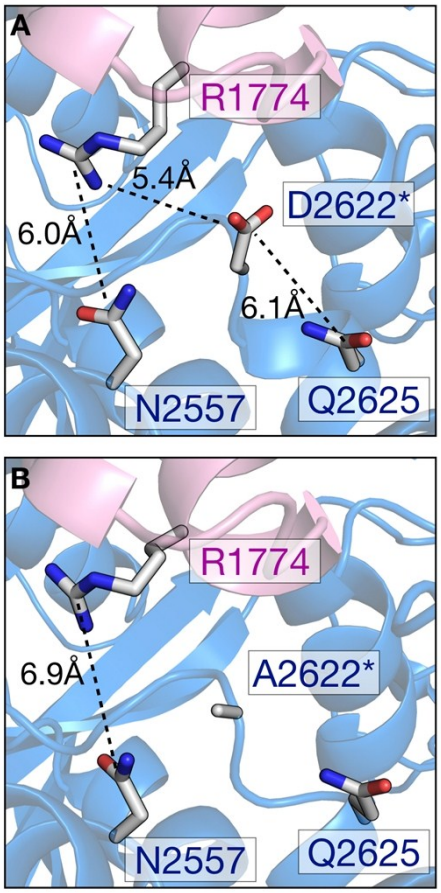

Figure SI12. Close-up of the interface across KS and ACP. KS, ACP residues and atom distances are highlighted in blue, magenta and black, respectively. Dashed lines indicate interaction between residues. The point mutation sites are marked with a star. (A) Wild-type interface with residues R1774, D2622 and Q2625. Two electrostatic interaction networks are observed between (i) R1774, N2557 (distance of 6.0 Å) and D2662 (5.4 Å) and (ii) D2662 and Q2625 (6.1 Å). (B) Mutant interface with residues R1774, A2622 and Q2625 is illustrated. The introduction of the apolar mutant disrupt the interactions between 1774, 2622 and 2625. The interaction between 1774 and 2557 is weakened (distance of 6.9 Å). The mutant interface is therefore expected to display a high (i.e., less favorable) relative binding energy than the wild-type model.

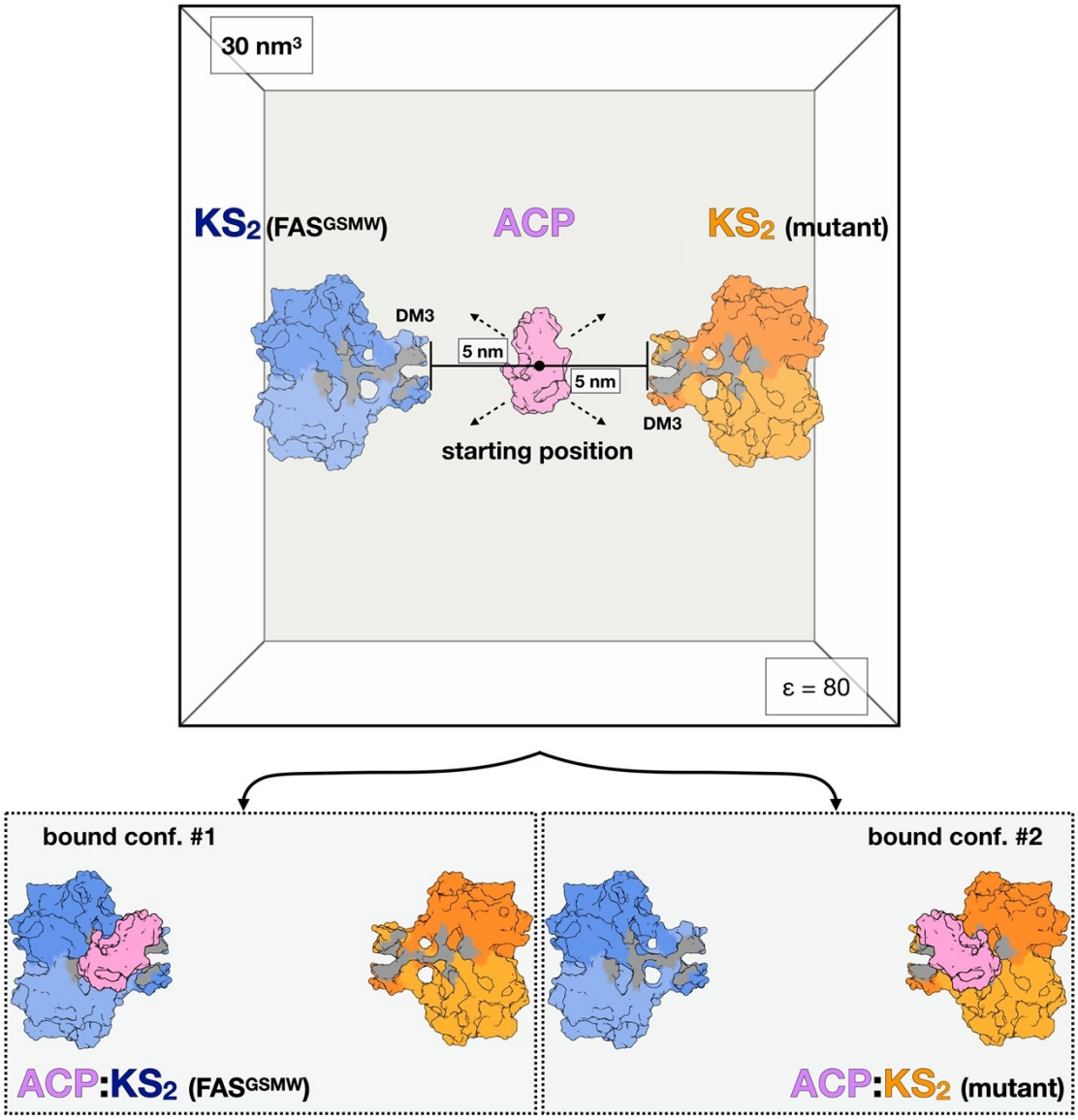

Figure SI13. Coarse-grained competitive scheme used to explore ACP:KS_2 binding. Wild type KS_2 of FAS^{GSMW} is illustrated in blue, and mutant KS_2 in orange. The interface residues of KS are highlighted in gray. ACP, illustrated in magenta, is placed at the center between the two KS dimers, separated by 5 Å from each dimer. One ACP initial position is illustrated here and the four investigated orientations of the carrier docking side are highlighted with black arrows. Two alternative bound conformations of ACP to KS are illustrated on the bottom.

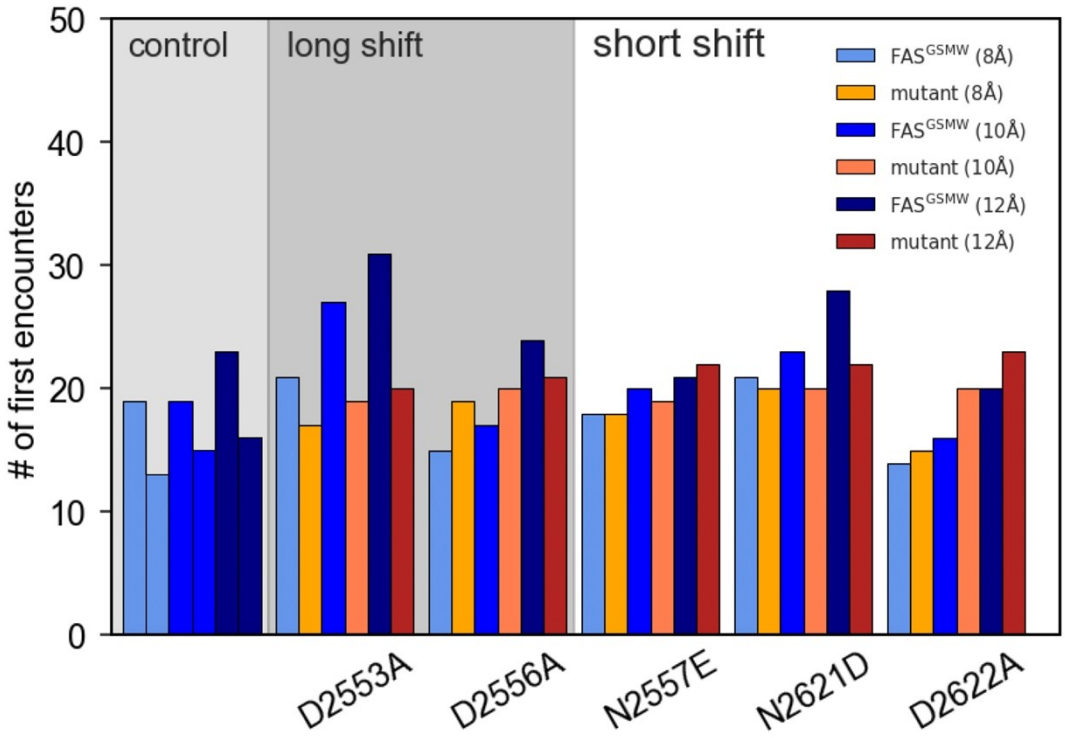

Figure SI14. Events of first encounters of ACP and KS_2 (vertical axis) calculated over 400 CG simulations for each construct (horizontal axis). Angstrom threshold refers to the distance between the active site Ser1772 (ACP) and the enzymatic DDI residue Ser2766.

Supporting Table 1. Overview of examined surface mutations. The mutation sites from this study are listed with the positions for *C. ammoniagenes* FAS (protein used for the presented *in vitro* study), for *S. cerevisiae* (from which the structure was used for rational planning) and for other proteins (which have previously been subject of ACP–domain interactions). For *S. cerevisiae* FAS, also the chain on which the mutation is located is listed in brackets.

	C. ammoniagenes	*S. cerevisiae*	Comments
KS domain	D2553	D1203 (α)	described mutation K63Q, FabB (*E. coli*)[40]
	D2556	S1206 (α)	described mutation K66Q, FabB (*E. coli*)[40]
	N2557	Q1207 (α)	similar to mutation K66Q, FabB (*E. coli*)[40]
	N2621	N1272 (α)	new in this study
	D2622	D1273 (α)	new in this study
	A2696	K1347 (α)	described mutation R206, FabF (*E. coli*) (0% binding)[41]
MPT domain	Q1647	R59 (α)	described mutation site R287, MCAT (*S. coelicolor*)[5]
	K1435	R1861 (β)	new in this study
	R1494	R1962 (β)	described mutation site R189, MCAT (*S. coelicolor*)
AT domain	I151A	I306A (β)	known from previous study[3]
	V289	I483 (β)	new in this study
	L290	I484 (β)	new in this study

Reference list:

1. Sumper, M.; Oesterhelt, D.; Riepertinger, C.; Lynen, F. *Eur. J. Biochem.* **1969,** *10* (2), 377-387.
2. Kawaguchi, A.; Arai, K.; Seyama, Y.; Yamakawa, T.; Okuda, S. *J. Biochem.* **1980,** *88* (2), 303-306.
3. Gajewski, J.; Buelens, F.; Serdjukow, S.; Janssen, M.; Cortina, N.; Grubmuller, H.; Grininger, M. *Nat. Chem. Biol.* **2017,** *13*, 363–365.
4. Gajewski, J.; Pavlovic, R.; Fischer, M.; Boles, E.; Grininger, M. *Nat. Commun.* **2017,** *8*, 14650.
5. Arthur, C. J.; Williams, C.; Pottage, K.; Ploskon, E.; Findlow, S. C.; Burston, S. G.; Simpson, T. J.; Crump, M. P.; Crosby, J. *ACS Chem. Biol.* **2009,** *4* (8), 625-636.
6. Rangan, V. S.; Smith, S. *J. Biol. Chem.* **1997,** *272* (18), 11975-11978.
7. Bunkoczi, G.; Misquitta, S.; Wu, X.; Lee, W. H.; Rojkova, A.; Kochan, G.; Kavanagh, K. L.; Oppermann, U.; Smith, S. *Chem. Biol.* **2009,** *16* (6), 667-675.
8. Leibundgut, M.; Jenni, S.; Frick, C.; Ban, N. *Science* **2007,** *316* (5822), 288-290.
9. Consortium, T. U. *Nucleic Acids Res.* **2017,** *45* (D1), D158-d169.
10. Buchan, D. W. A.; Minneci, F.; Nugent, T. C. O.; Bryson, K.; Jones, D. T. *Nucleic Acids Res.* **2013,** *41* (W1), W340-W348.
11. Kim, Y. C.; Hummer, G. *J. Mol. Biol.* **2008,** *375* (5), 1416-1433.
12. Jenni, S.; Leibundgut, M.; Boehringer, D.; Frick, C.; Mikolasek, B.; Ban, N. *Science* **2007,** *316* (5822), 254-261.
13. Lomakin, I. B.; Xiong, Y.; Steitz, T. A. *Cell* **2007,** *129* (2), 319-332.
14. Gowers, R. J.; Linke, M.; Barnoud, J.; Reddy, T. J. E.; Melo, M. N.; Seyler, S. L.; Dotson, D. L.; Domanski, J.; Buchoux, S.; Kenney, I. M.; Beckstein, O. *Proceedings of the 15th Python in Science Conference* **2016**, 102-109.
15. Michaud-Agrawal, N.; Denning, E. J.; Woolf, T. B.; Beckstein, O. *J. Comput. Chem.* **2011,** *32* (10), 2319-2327.
16. Jones, E.; Oliphant, E.; Peterson, P. http://www.scipy.org/ [Online, accessed 2018-07-11].
17. Enderle, M.; McCarthy, A.; Paithankar, K. S.; Grininger, M. *Acta Crystallogr. F Struct. Biol. Commun.* **2015,** *71* (Pt 11), 1401-7.
18. Schmidt, T.; Skerra, A. *Nat. Protoc.* **2007,** *2* (6), 1528-1535.
19. Boehringer, D.; Ban, N.; Leibundgut, M. *J. Mol. Biol.* **2013,** *425* (5), 841-849.
20. Katoh, K.; Standley, D. M. *Mol. Biol. Evol.* **2013,** *30* (4), 772-80.
21. Henikoff, S.; Henikoff, J. G. *Proc. Natl. Acad. Sci. U. S. A.* **1992,** *89* (22), 10915-10919.
22. Waterhouse, A. M.; Procter, J. B.; Martin, D. M.; Clamp, M.; Barton, G. J. *Bioinformatics* **2009,** *25* (9), 1189-1191.
23. Sali, A.; Blundell, T. L. *J. Mol. Biol* **1993,** *234*, 779-815.
24. Chan, D. I.; Stockner, T.; Tieleman, D. P.; Vogel, H. J. *J. Biol. Chem.* **2008**, *283*, 33620.
25. Roujeinikova, A.; Simon, W. J.; Gilroy, J.; Rice, D. W.; Rafferty, J. B.; Slabas, A. R. *J. Mol. Biol.* **2007**, *365*, 135.
26. Perez, D. R.; Leibundgut, M.; Wider, G. *Biochem.* **2015**, *54*, 2205.
27. Pettersen, E. F.; Goddard, T. D.; Huang, C. C.; Couch, G. S.; Greenblatt, D. M.; Meng, E. C.; Ferrin, T. E., UCSF Chimera--a visualization system for exploratory research and analysis. *J. Comput. Chem.* **2004,** *25* (13), 1605-1612.
28. Berendsen, H. J. C.; van der Spoel, D.; van Drunen, R. *Comput. Phys. Commun.* **1995,** *91* (1-3), 43-56.
29. Brooks, B. R.; Brooks, C. L., 3rd; Mackerell, A. D., Jr.; Nilsson, L.; Petrella, R. J.; Roux, B.; Won, Y.; Archontis, G.; Bartels, C.; Boresch, S.; Caflisch, A.; Caves, L.; Cui, Q.; Dinner, A. R.; Feig, M.; Fischer, S.; Gao, J.; Hodoscek, M.; Im, W.; Kuczera, K.; Lazaridis, T.; Ma, J.; Ovchinnikov, V.; Paci, E.; Pastor, R. W.; Post, C. B.; Pu, J. Z.; Schaefer, M.; Tidor, B.; Venable, R. M.; Woodcock, H. L.; Wu, X.; Yang, W.; York, D. M.; Karplus, M. *J. Comput. Chem.* **2009,** *30* (10), 1545-1614.
30. Huang, J.; MacKerell, A. D., Jr. *J. Comput. Chem.* **2013,** *34* (25), 2135-2145.
31. Bussi, G.; Donadio, D.; Parrinello, M. *J. Chem. Phys.* **2007,** *126* (1), 014101.
32. Parrinello, M.; Rahman, A. *J. Appl. Phys.* **1981,** *52* (12), 7182-7190.
33. Humphrey, W.; Dalke, A.; Schulten, K. *J. Mol.Graph.* **1996,** *14* (1), 33-8, 27-8.
34. Kumari, R.; Kumar, R.; Lynn, A. *J. Chem. Inf. Model.* **2014,** *54* (7), 1951-1962.
35. Baker, N. A.; Sept, D.; Joseph, S.; Holst, M. J.; McCammon, J. A. *Proc. Natl. Acad. Sci. U. S. A.* **2001,** *98* (18), 10037-10041.
36. Lee, B.; Richards, F. M. *J. Mol. Biol.* **1971,** *55* (3), 379-400.
37. Shrake, A.; Rupley, J. A. *J. Mol. Biol.* **1973,** *79* (2), 351-371.
38. Schweizer, E.; Hofmann, J. *Microbiol. Mol. Biol. Rev.* **2004,** *68* (3), 501-517.
39. Sievers, F.; Wilm, A.; Dineen, D.; Gibson, T. J.; Karplus, K.; Li, W.; Lopez, R.; McWilliam, H.; Remmert, M.; Söding, J.; Thompson, J. D.; Higgins, D. G. *Mol. Syst. Biol.* **2011,** *7* (539), 1-6.
40. Borgaro, J. G.; Chang, A.; Machutta, C. A.; Zhang, X.; Tonge, P. J. *Biochem.* **2011,** *50* (49), 10678-10686.
41. Ye, Z.; Williams, G. J. *Biochem.* **2014,** *53* (48), 7494-7502.